APL Materials

RESEARCH ARTICLE | JUNE 01 2023

CrB-type, ordered *α*-MnB: Single crystal structure and spin-canted magnetic behavior

Special Collection: Challenges and Perspectives in Materials Chemistry—A Celebration of Prof. Sir Anthony K. Cheetham's 75th Birthday

Nalan Kalyon ; Anne-Marie Zieschang; Kathrin Hofmann ; Maren Lepple ; Maximilian Fries ; Konstantin P. Skokov ; Michael Dürrschnabel; Hans-Joachim Kleebe; Oliver Gutfleisch ; Barbara Albert

APL Mater 11, 060701 (2023)
https://doi.org/10.1063/5.0148236

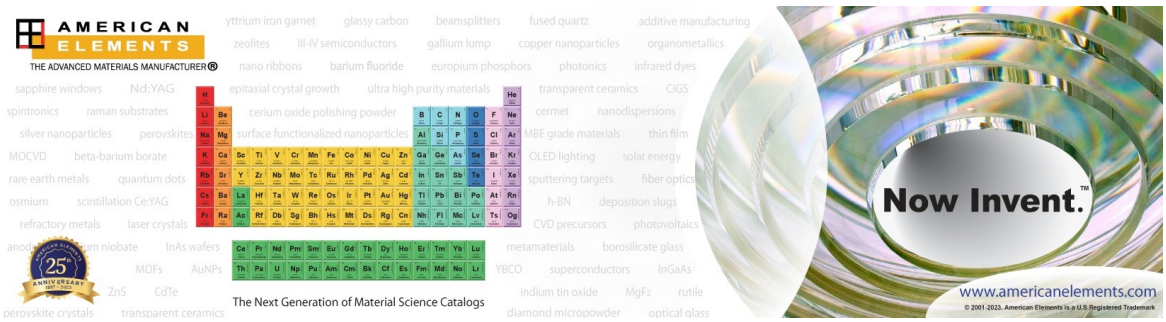

CrB-type, ordered α-MnB: Single crystal structure and spin-canted magnetic behavior

Cite as: APL Mater. 11, 060701 (2023); doi: 10.1063/5.0148236
Submitted: 28 February 2023 • Accepted: 10 May 2023 •
Published Online: 1 June 2023

Nalan Kalyon,[1] Anne-Marie Zieschang,[1] Kathrin Hofmann,[1] Maren Lepple,[1,a)] Maximilian Fries,[2] Konstantin P. Skokov,[2] Michael Dürrschnabel,[3,b)] Hans-Joachim Kleebe,[3] Oliver Gutfleisch,[2] and Barbara Albert[1,c)]

AFFILIATIONS

[1] Eduard-Zintl-Institute of Inorganic and Physical Chemistry, Technische Universität Darmstadt, Peter-Grünberg-Str. 12, 64287 Darmstadt, Germany
[2] Institute of Materials Science, Technische Universität Darmstadt, Peter-Grünberg-Str. 16, 64287 Darmstadt, Germany
[3] Department of Materials and Earth Sciences, Electron Microscopy Center Darmstadt (EMC-DA), Technische Universität Darmstadt, Peter-Grünberg-Str. 2, 64287 Darmstadt, Germany

Note: This paper is part of the Special Topic on Challenges and Perspectives in Materials Chemistry—A Celebration of Prof. Sir Anthony K. Cheetham's 75th Birthday.

[a)] **Now at:** Institute of Inorganic and Analytical Chemistry, Justus Liebig University Gießen, Heinrich-Buff-Ring 17, 35392 Gießen, Germany.
[b)] **Now at:** Institute for Applied Materials, Karlsruhe Institute of Technology, Hermann-von-Helmholtz-Platz 1, 76344 Eggenstein-Leopoldshafen, Germany.
[c)] **Author to whom correspondence should be addressed:** barbara.albert@tu-darmstadt.de. **Now at** University Duisburg-Essen.

ABSTRACT

Manganese monoboride has a low- (α) and a high-temperature (β) modification, as well as a defect-rich low-temperature variant (α'). The crystal structure (FeB-type structure, s.g. *Pnma*) and properties of high-temperature MnB are well-known. In this work, single crystals were grown via chemical vapor transport reactions, both of β-MnB and the low-temperature modification, α-MnB. This allowed for determining the crystal structure of defect-free α-MnB [CrB-type structure, s.g. *Cmcm*, a = 3.0098(6) Å, b = 7.6390(2) Å, and c = 2.94620(6) Å]. Furthermore, α'-MnB, the stacking fault-dominated CrB-variant, was obtained as crystalline powder and characterized by X-ray powder diffraction and transmission electron microscopy. Direction-resolved measurements of the magnetic properties of α-MnB revealed spin-canted magnetic behavior along c and ferromagnetism along a and b with a Curie temperature of 456 K; ferromagnetic β-MnB has a Curie temperature of 568 K.

I. INTRODUCTION

There are more than 1000 binary boron compounds, accessible through different synthesis methods.[1–3] Borides are generally known for properties like chemical inertness, heat and wear resistivity, hardness, and interesting magnetic behavior.[2–5] Some prominent examples are MgB_2 as a superconductive material with a high critical temperature of 39 K,[6] ReB_2 as an inorganic diamond,[7] MoB_2,[8] Ni_3B,[9] (Co, Fe)$_2$B,[10,11] and Co_3B[12] as electrocatalysts, and Co_2B and Ni_7B_3[13] as catalysts for the selective hydrogenation of citral.[14] As pointed out by Bocarsly *et al.*,[15] compounds like MnB with strongly coupled magnetic and structural transitions can be of interest for energy-efficient and environmentally friendly refrigerators, heat pumps, and thermomagnetic generators. Only recently, Ma *et al.* described MnB as promising material because it is incompressible and ferromagnetic at the same time.[16]

Six binary manganese borides have been described in the literature: Mn_2B, MnB, Mn_3B_4, MnB_2, MnB_4, and MnB_{23}.[17–25] Manganese monoboride crystallizes in two different structure types. The low-temperature modification was reported to crystallize with a CrB-type structure (α-MnB, s.g. *Cmcm*), and the high-temperature modification was reported to crystallize with a FeB-type structure

TABLE I. Synthesis parameters of the chemical vapor transport reaction of manganese monoboride.

Product	T/K	Duration/days	Form of product
α'-MnB	1073	14	Powder
α-MnB	1223	21	Powder and crystals
β-MnB	1423	14	Powder and crystals

(β-MnB, s.g. *Pnma*).[15,16,19,23] Different synthesis methods for the high-temperature modification of MnB are known.[15,26–29] β-MnB is ferromagnetic and has the highest magnetic moment per metal atom (1.92 μ_B) of all transition metal monoborides.[26,27,30–32] This makes it a promising material for applications such as magnetocaloric and magnetic hyperthermia.[15] Papesch *et al.*[33] reported α-MnB for the first time. Smid *et al.*[23] obtained single crystals of this modification. α-MnB was reported to be stable below 1223 K and β-MnB between 1373 and 1473 K. The defect structure of nanoscale manganese monoboride, α'-MnB, was described by Klemenz *et al.*[34] with a saturation magnetization of 80 $Am^2\ kg^{-1}$ at 100 K and a Curie temperature of 545 K. Ma *et al.*[16] obtained a similar substance via high-pressure synthesis. A similar modification of nanoscale FeB containing stacking faults is also known,[35,36] and its crystal structure was recently described.[37]

While there are calculations and measurements of the magnetic behavior of β-MnB,[15,26,27,32,38,39] the magnetic and other physical properties of α-MnB single crystals were previously unknown and will be reported here.

II. EXPERIMENTAL DETAILS

A. Synthesis

Manganese pieces (chemPUR, >99.9%) and crystalline boron powder (chemPUR, >99.95%) were weighed in stoichiometric ratios with a 10% excess of manganese due to the formation of MnI_2. To obtain the α'- and β-modifications, the starting materials were homogenized in a tungsten carbide ball mill prior to chemical vapor transport. The elements were placed in a half ampoule for preheating under vacuum at 1073 K for two hours. Iodine was added as a mineralizing agent. The quartz ampoule was sealed under vacuum and heated. Table I gives further details. The ampoule was quenched after the heat treatment.

B. Structural characterization

Microcrystalline powders were characterized using X-ray diffraction (XRD) on a powder diffractometer (STADI P, STOE&Cie GmbH, Darmstadt) with Debye–Scherrer geometry at room temperature. For α- and β-MnB, copper radiation was used [Cu Kα_1, λ = 1.540 60 Å, Ge(111) monochromator, 2θ range of 10° to 90°, Mythen detector, glass capillary]. α'-MnB was investigated using molybdenum radiation [Mo Kα_1, λ = 0.709 30 Å, Ge(111) monochromator, 2θ range of 5° to 50°, position sensitive detector, acetate film]. Rietveld refinement was performed using the program TOPAS.[40]

The structure of the single crystals was determined using a single crystal diffractometer (IPDS 2 STOE&Cie GmbH, Darmstadt). The measurement was performed with molybdenum radiation (MoK$_\alpha$, λ = 0.710 73 Å) at room temperature. Structure solution and refinement of the lattice parameters and atom positions were subsequently done using the program SHELX-97.[41]

TABLE II. Single crystal structure analysis of α-MnB and β-MnB.

	α-MnB	β-MnB
Radiation	Mo Kα, λ = 0.710 73 Å	
Crystal system	Orthorhombic	Orthorhombic
Space group	*Cmcm* (no. 63)	*Pnma* (no. 62)
a/Å	3.0098(6)	5.5389(2)
b/Å	7.6390(2)	2.9622(6)
c/Å	2.9420(6)	4.1266(8)
V/Å^3	67.64(2)	67.71(2)
Z	4	4
ρ/g cm^{-3}	6.456	6.450
Collected reflections	596	1114
Independent reflections	62	107
θ-range/°	5.35–28.89	6.16–29.06
GOF	1.34	1.17
R_1	0.0136	0.0479
wR_2	0.0299	0.1092

C. Magnetic measurements

Magnetic measurements of the single crystals of α- and β-MnB were performed using a Physical Property Measurement System (14T PPMS, Quantum Design) with a vibrating sample magnetometer (VSM) option. To measure the magnetic saturation of the different crystallographic axes, isothermal $M(H)$ scans at 10 to 300 K were measured from 0 to 4 T. $M(T)$ measurements were collected using a VSM (LakeShore VSM). For α'-MnB powder,

TABLE III. Atom positions and displacement parameters from the single crystal structure refinements of α-MnB and β-MnB.

	Atom	Wyckoff position	x/a	y/b	z/c	U_{eq}/Å^2
α-MnB	Mn1	4c	0	0.1437(6)	0.25	0.0060(3)
	B1	4c	0	0.4328(6)	0.25	0.0083(7)
β-MnB	Mn1	4c	0.1762(1)	0.25	0.1206(7)	0.0049(6)
	B1	4c	0.0312(2)	0.25	0.6133(2)	0.0082(2)

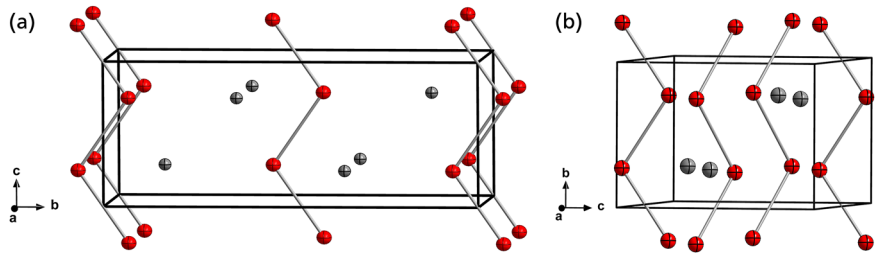

FIG. 1. Crystal structures of (a) α-MnB (CrB-type structure) and (b) β-MnB (FeB-type structure), red: B and gray: Mn. Atoms are drawn with an 80% probability of anisotropic displacement ellipsoids.

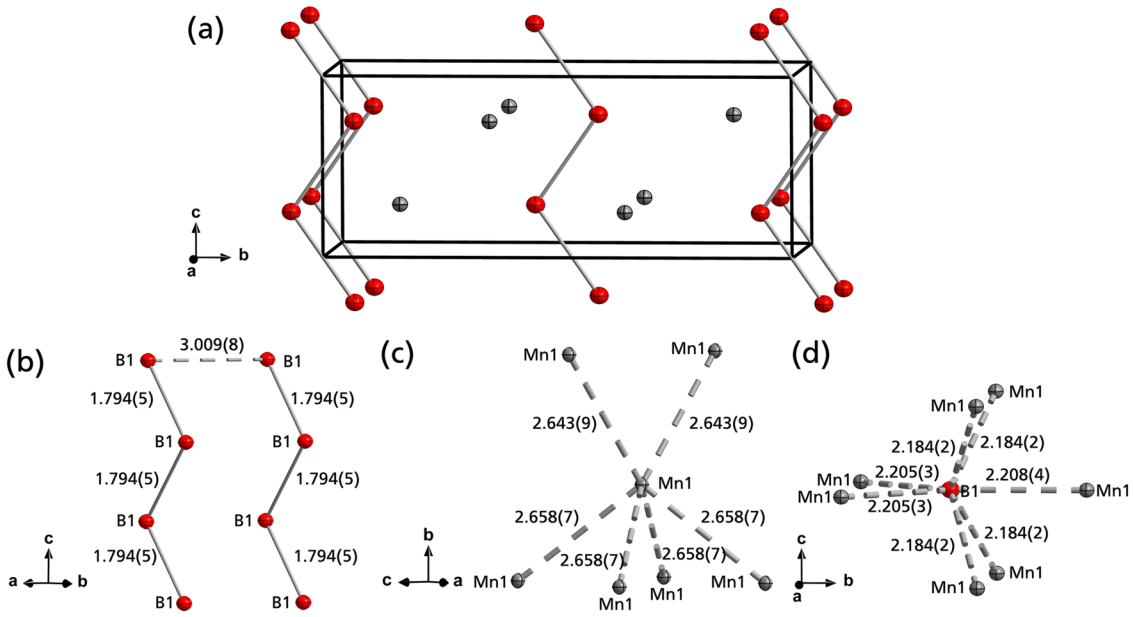

FIG. 2. Unit cell (a), and bond lengths and distances between atoms (b)–(d) in the structure of α-MnB (red: B and gray: Mn).

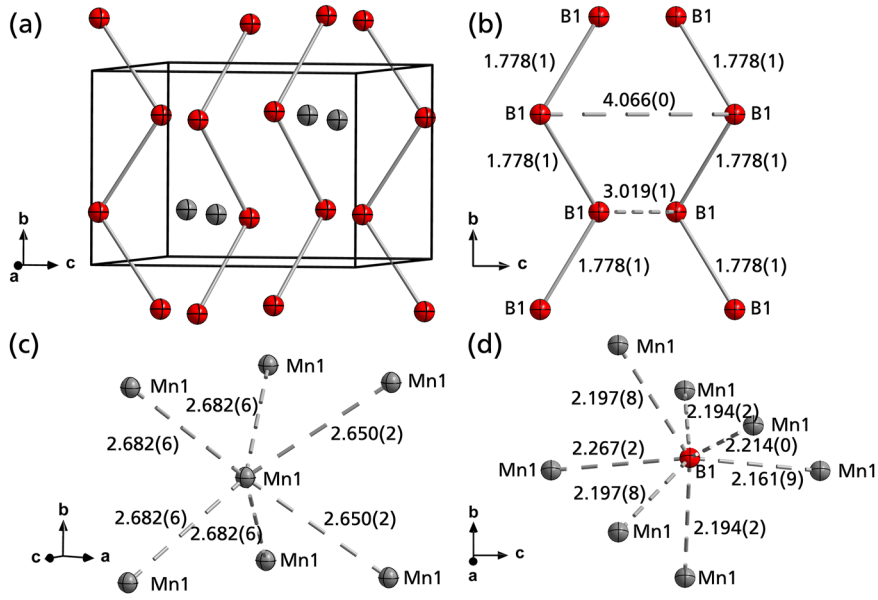

FIG. 3. Unit cell (a), and bond lengths and distances between atoms (b)–(d), in the structure of β-MnB (red: B and gray: Mn).

isofield $M(H)$ measurements were collected between 350 and 600 K at magnetic fields of 0.1, 1, and 2 T. Additionally, isothermal $M(H)$ measurements between 10 and 560 K were collected.

D. Differential scanning calorimetry

Calorimetric measurements were run using a high temperature differential scanning calorimeter (STA 449 F3 Jupiter, Netzsch). 30 to 50 mg of the polycrystalline powder of manganese monoboride were placed in a BN-crucible. α-MnB was measured in a temperature range of 313 to 533 K, and β-MnB was measured between 313 and 783 K. The heat capacities of the two modifications were measured between 323 and 673 K. Sapphire was used as a standard.

E. Microscopy

The single crystals were imaged using a digital microscope (VHX 500F, Keyence). For capturing the morphology of the crystals of manganese monoboride, scanning electron microscopy (SEM, JEOL, JSM 6400, 20 kV) was used. The material was placed on a carbon pad. To verify the stacking faults of α'-MnB, a (scanning) transmission electron microscope (STEM, JEOL, ARM-200F, 120 kV) was used. High-angle annular dark field (HAADF) and annular bright-field (ABF) images were recorded.

F. Analysis of density

The density of the materials was measured using the gas pycnometric density method (Accupyc 1340, Micromeritics) at room temperature. The specimen with a known mass was placed in the chamber and flooded with helium. The density of the sample was determined after measuring the volume of the chamber.

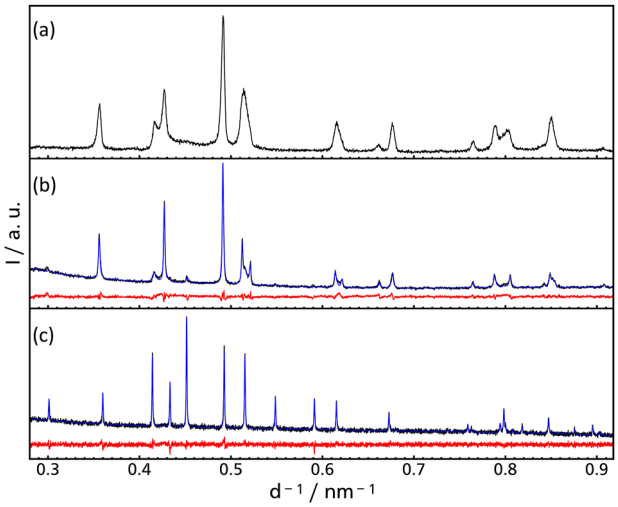

FIG. 6. Powder diffraction patterns of (a) α'-MnB and (b) α-MnB as well as (c) β-MnB (black: measured, blue: calculated, and red: difference).

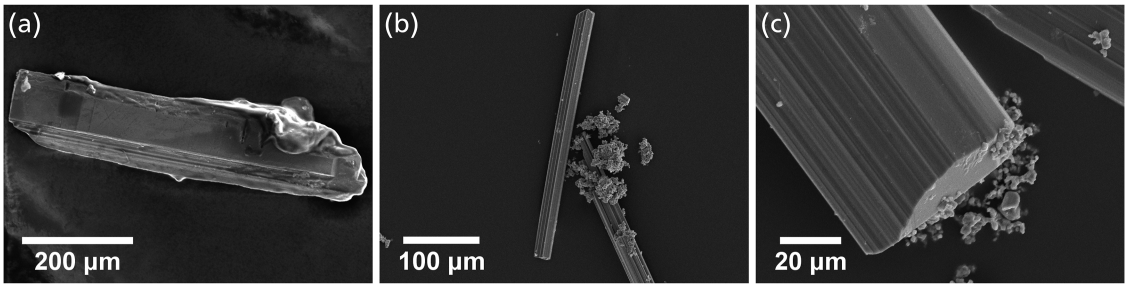

FIG. 4. Scanning electron microscopy images of (a) α-MnB, and (b) and (c) β-MnB.

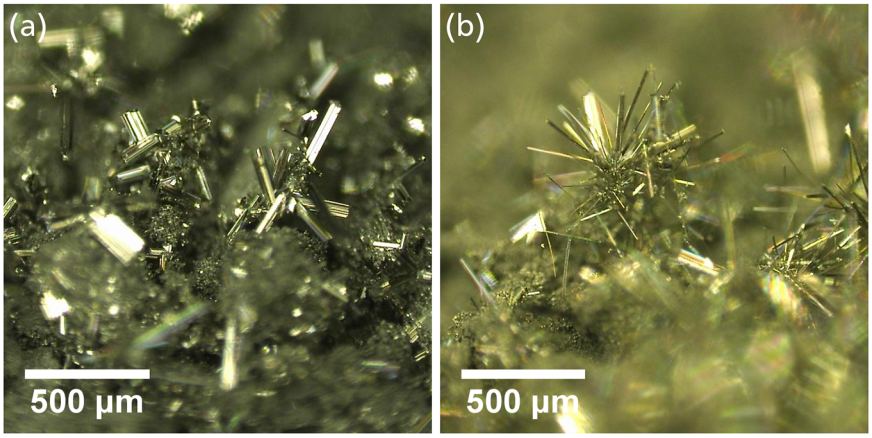

FIG. 5. Optical appearance of (a) α-MnB and (b) β-MnB.

III. RESULTS AND DISCUSSION

By chemical vapor transport reactions, crystals of two different modifications of MnB were obtained. Solving the crystal structure was possible using direct methods for α-MnB and β-MnB. The results of the crystallographic information for α-MnB and β-MnB are given in Tables II and III.[42]

α-MnB crystallizes in the orthorhombic crystal system (s.g. *Cmcm*) with a CrB-type structure. Boron atoms form zigzag chains that are orientated parallel to the *c* axis, whereas the manganese atoms are isolated between the boron zigzag chains. β-MnB crystallizes in the orthorhombic crystal system (s.g. *Pnma*) with a FeB-type structure. The boron atoms form zigzag chains along the *b* axis with isolated manganese atoms between them. The unit cells of α-MnB and β-MnB are shown in Figs. 1(a) and 1(b). The pycnometric densities of α-MnB and β-MnB were determined to be 6.446 and 6.241 g cm^{-3} and were comparable to the crystallographic densities of 6.456 and 6.450 g cm^{-3}.

The bond lengths and distances between atoms are given in Figs. 2(b)–2(d) and Figs. 3(b)–3(d) for α-MnB and β-MnB, respectively. The B–B bond in α-MnB is 1.794(5) Å. The B–B distance between the chains is 3.009(8) Å. For β-MnB, the B–B bond is 1.778(1) Å and the B–B distances between the neighboring chains are 4.066(0) and 3.019(1) Å. The Mn–Mn distances are nearly the same: 2.643(9) and 2.658(7) Å for α-Mn, and 2.682(6) and 2.650(2) Å for β-MnB. The Mn–B distances range from 2.184(2) to 2.208(4) Å in α-MnB and from 2.161(9) to 2.267(2) Å in β-MnB.

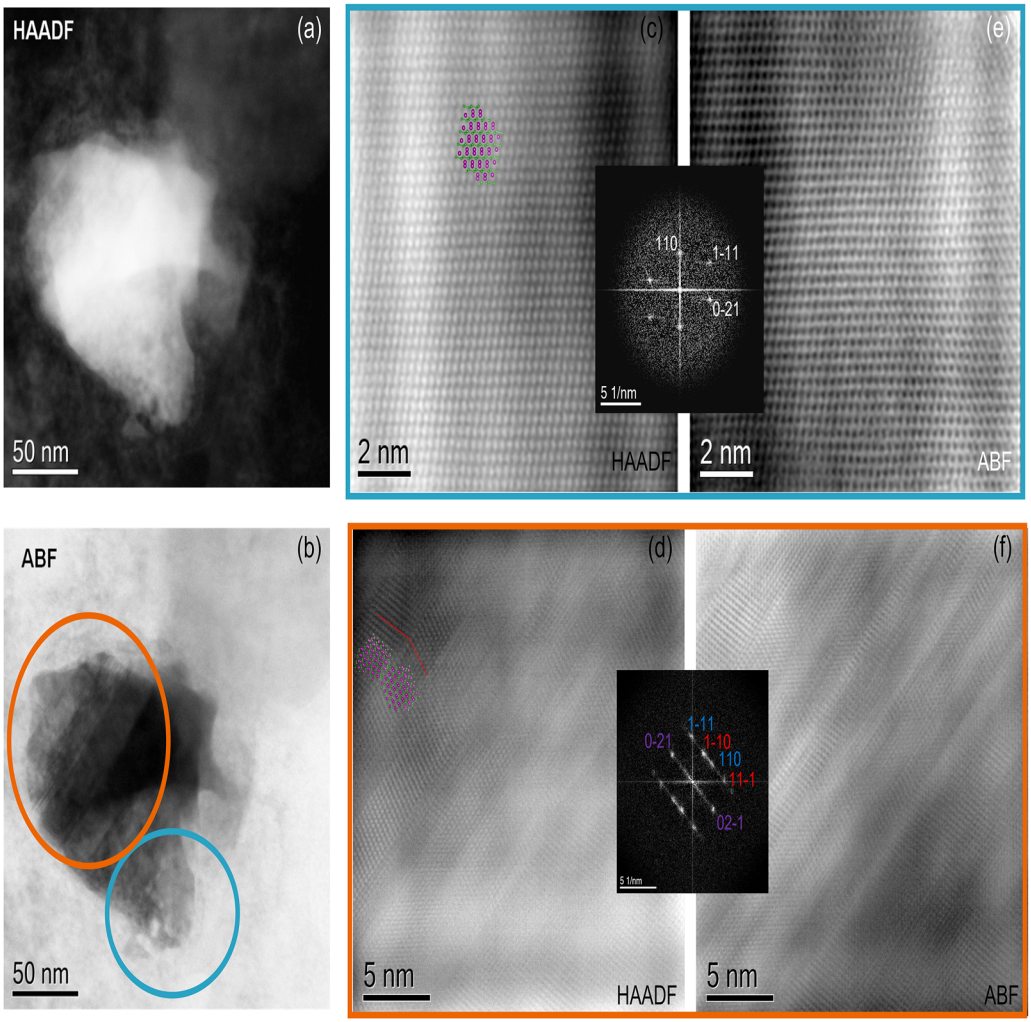

FIG. 7. (a) High-angle annular dark-field and (b) annular bright-field transmission electron microscopy images of α'-MnB. Atomic resolution scanning transmission electron microscopy images of (c) and (e) an ordered region (blue) and (d) and (f) a region, which contains stacking faults (orange), of α'-MnB. The insets in both boxes show the FFT of the HAADF image, respectively. In the disordered region, nanotwins are present. The twin plane is (0-21), and red indices correspond to a [112] and blue indices to a [−112] zone-axis orientation.

Scanning electron microscope images of the single crystals obtained by chemical vapor transport reaction are shown in Figs. 4(a)–4(c). Figures 5(a) and 5(b) give an impression of their optical appearance shown by digital microscopy and also show that single crystals were grown from a matrix of crystalline powder. α-MnB crystals were rod-shaped and 300–500 μm in length, and β-MnB crystals were needle-shaped and 300–400 μm in length.

Powder patterns of the three phases obtained by chemical vapor transport reactions are given in Fig. 6. A phase-pure sample of β-MnB was obtained. Crystalline powders of α-MnB contained 1 wt. % β-Mn as a side-phase. The lattice parameters were refined using the Rietveld method (supplementary material, Tables S1 and S2) and found to be comparable to our single crystal data and the literature data.[19,33] The powder pattern of α'-MnB was comparable to those of the defect-rich phases described earlier by Kanaizuka *et al.*,[43] Klemenz *et al.*,[34] and Ma *et al.*[16]

Transmission electron microscopy images recorded at 373 K confirm the presence of stacking faults in α'-MnB. In Figs. 7(a) and 7(b), high-angle annular dark-field and annular bright-field images of a particle that consists of a region that is ordered (blue) and a region that contains stacking faults and nanotwins (orange box) are shown. An atomic resolution HAADF and bright-field images of an ordered region are shown in Figs. 7(c) and 7(e). The inset shows the FFT of the HAADF image. An atomic model of α-MnB in [−112] zone axis orientation was overlaid for interpreting the image contrast. An atomic resolution HAADF and bright-field images of an ordered region are shown in Figs. 7(d) and 7(f). An atomic model was overlaid to highlight the presence of nanotwins in the left upper image quadrant of Fig. 7(d). The FFT image is shown as an inset in the orange box of Fig. 7. The presence of nanotwins requires the use of two crystal orientations for indexing the FFT, i.e., the [112] zone-axis orientation in red color and the [−112] zone-axis orientation in

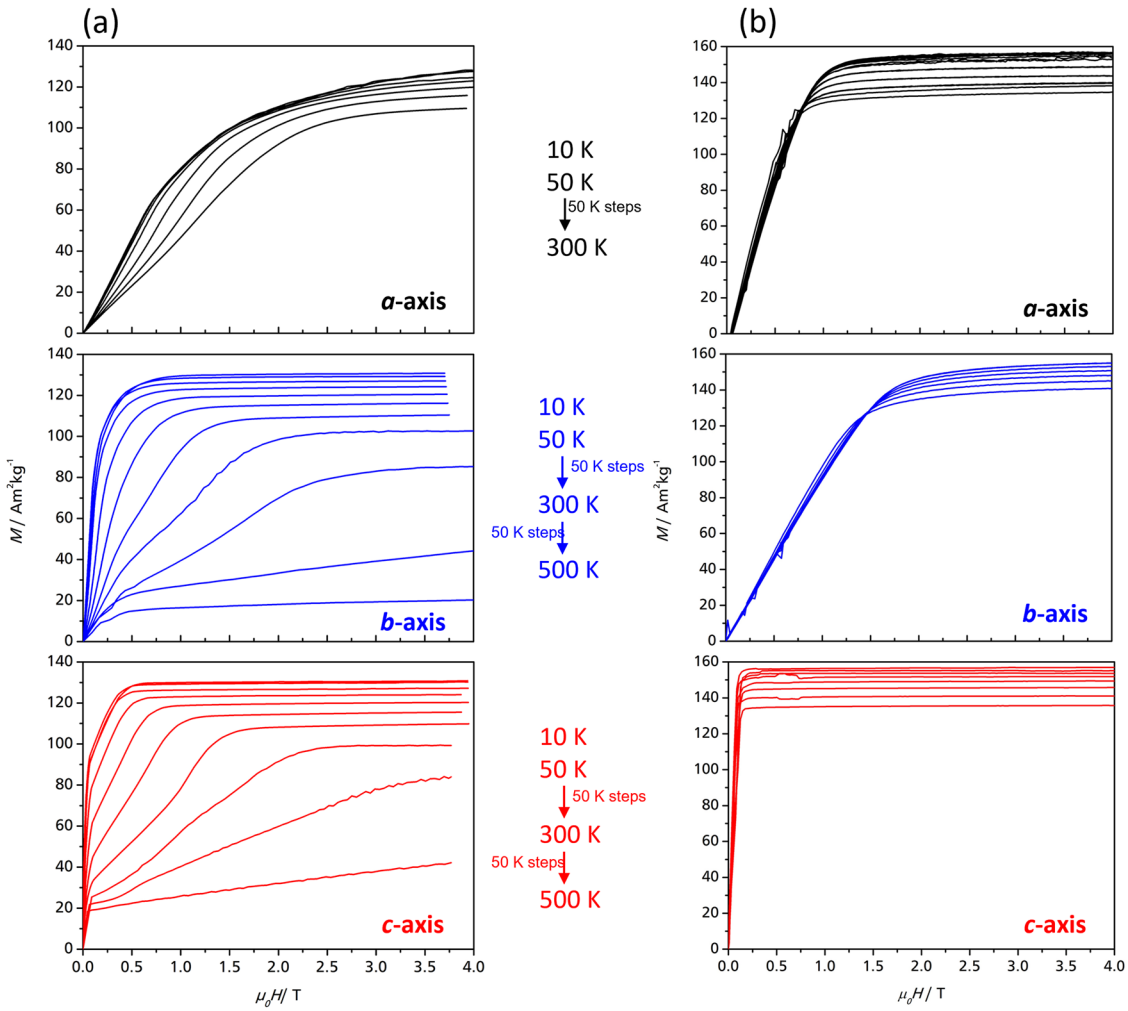

FIG. 8. Isothermal $M(H)$ measurements of single crystals of (a) α-MnB and (b) β-MnB along the different crystallographic axes (black: *a*, blue: *b*, and red: *c*) collected at 10 K (top) and between 50 and 300 K in steps of 50 K (from top to bottom). Additional high-temperature measurements are shown for the *b* and *c* axes of α-MnB between 350 and 500 K in steps of 50 K.

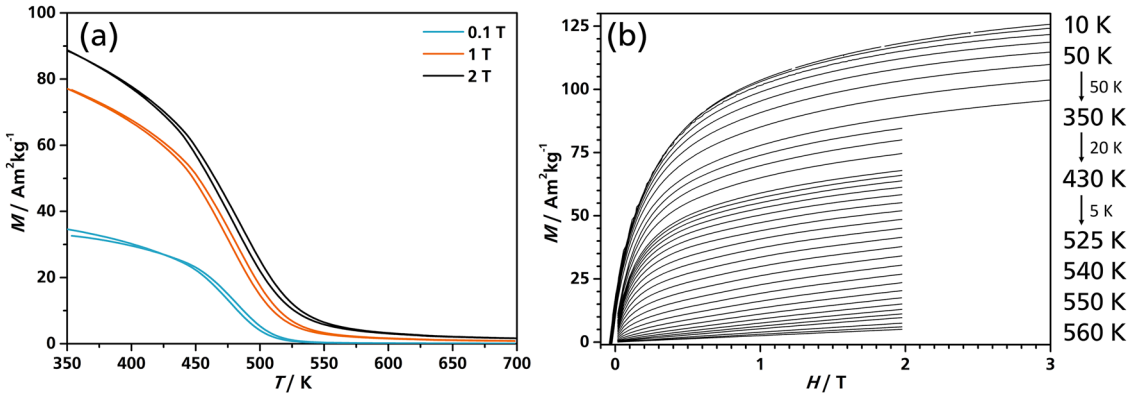

FIG. 9. $M(T)$ and $M(H)$ measurements of α'-MnB powder. (a) Isofield $M(T)$ measurements at 0.1 T (blue), 1 T (orange), and 2 T (black). (b) Isothermal $M(H)$ measurements collected at 10 K (top) to 560 K (bottom).

blue color. The common twin plane is the {0-21}-type plane. Thus, these type indices are given in violet color. Besides the nanotwins, stacking faults of the {0-21}-planes are present as can be seen from the streaking along that direction.

Results from magnetic measurements along the different crystallographic axes of α-MnB and β-MnB single crystals are shown in Fig. 8. α-MnB has ferromagnetic behavior along [100] and [010]. The measurements along [001] showed unexpected magnetic behavior even at high temperatures (500 K). This phenomenon may be attributed to so-called spin-canted magnetism.[44] At low magnetic fields the spins are neither perpendicular nor parallel to the c axis. When the magnetic field is increased, the spins slowly align with the magnetic field. This process is independent of temperature. The saturation magnetization of α-MnB was determined to be 130 $Am^2\ kg^{-1}$ at 10 K (1.54 μ_B/Mn).

Magnetic measurements of β-MnB on very thin, needle-like single crystals were difficult but confirmed its ferromagnetic behavior as shown earlier.[15,26–29] β-MnB showed magnetic anisotropy and a saturation magnetization of 156 $Am^2\ kg^{-1}$ (1.84 μ_B/Mn) at 10 K.

Magnetic investigations of powders of α'-MnB led to results shown in Fig. 9. The Curie temperature determined by isofield $M(T)$ measurements [Fig. 9(a)] is 500 K. Isothermal low-temperature and high-temperature $M(H)$ measurements were collected between 0 and 3 T or 0 and 2 T, respectively [Fig. 9(b)]. The saturation magnetization was determined to be 124 $Am^2\ kg^{-1}$ at 10 K.

Differential scanning calorimetry (DSC) measurements were performed to investigate the ferromagnetic to the paramagnetic transition of MnB (supplementary material, Fig. S1). The transition temperature was determined to be 456 K for α-MnB and 574 K for β-MnB. The process was reversible for both modifications. The value for β-MnB is comparable to the Curie temperature described in the literature.[15,26,27,29]

IV. CONCLUSIONS

Chemical vapor transport reactions between manganese and boron in the presence of traces of iodine allowed the growth and structural characterization of single crystals of β- and α-manganese monoboride as well as the preparation of crystalline powders of these two phases and in addition of α'-MnB, a stacking-fault dominated variant that was earlier described either as α or α'. Due to the combination of X-ray diffraction and transmission electron microscopy, a clear differentiation between ordered α-MnB and defect-rich α'-MnB was possible for the first time. Magnetic measurements on single crystals allowed for the first description of temperature-dependent anisotropic magnetic properties of β- and α-manganese monoboride. Spin-canted magnetism was observed for α-MnB. Curie temperatures and phase transition temperatures were determined. Compounds like MnB with strongly coupled magnetic and structural transitions are of interest for magnetocaloric applications.

SUPPLEMENTARY MATERIAL

supplementary material is available under [link], including data on Rietveld refinements of α- and β-MnB (Tables S1 and S2) as well as anisotropic components of the displacement parameters from the single crystal structure determination of the α-modification (Table S3). Furthermore, DSC traces are given for both modifications (Fig. S1).

ACKNOWLEDGMENTS

We gratefully thank the German federal state of Hesse through its excellence program LOEWE "RESPONSE" for the financial support.

AUTHOR DECLARATIONS

Conflict of Interest

The authors have no conflicts to disclose.

Author Contributions

Nalan Kalyon: Data curation (equal); Formal analysis (equal); Investigation (equal); Writing – original draft (equal); Writing –

review & editing (equal). **Anne-Marie Zieschang**: Formal analysis (equal); Investigation (equal); Validation (equal); Visualization (equal); Writing – original draft (equal); Writing – review & editing (equal). **Kathrin Hofmann**: Conceptualization (equal); Data curation (equal); Formal analysis (equal); Methodology (equal). **Maren Lepple**: Data curation (equal); Formal analysis (equal); Investigation (equal); Methodology (equal). **Maximilian Fries**: Data curation (equal); Investigation (equal). **Konstantin P. Skokov**: Validation (equal). **Michael Dürrschnabel**: Data curation (equal); Formal analysis (equal); Investigation (equal). **Hans-Joachim Kleebe**: Supervision (equal). **Oliver Gutfleisch**: Funding acquisition (equal); Supervision (equal). **Barbara Albert**: Conceptualization (equal); Supervision (equal); Writing – original draft (equal); Writing – review & editing (equal).

DATA AVAILABILITY

The data that support the findings of this study are available within the article and its supplementary material.

REFERENCES

[1] G. Akopov, M. T. Yeung, and R. B. Kaner, "Rediscovering the crystal chemistry of borides," Adv. Mater. **29**, 1604506 (2017).

[2] B. P. T. Fokwa, "Borides: Solid-state chemistry," Encycl. Inorg. Bioinorg. Chem. **1**, 1–14 (2014).

[3] V. I. Matkovich, *Boron and Refractory Borides* (Springer-Verlag, Berlin, 1977).

[4] B. Albert and H. Hillebrecht, "Boron: Elementary challenge for experimenters and theoreticians," Angew. Chem., Int. Ed. **48**, 8640–8668 (2009).

[5] B. Aronsson, T. Lundström, and S. Rundqvist, *Borides, Silicides and Phosphides* (John Wiley & Sons Ltd., New York, 1965).

[6] J. Nagamatsu, N. Nakagawa, T. Muranaka, Y. Zenitani, and J. Akimitsu, "Superconductivity at 39 K in magnesium diboride," Nature **410**, 63–64 (2001).

[7] R. B. Kaner, J. J. Gilman, and S. H. Tolbert, "Designing superhard materials," Science **308**, 1268–1269 (2005).

[8] H. Park, A. Encinas, J. P. Scheifers, Y. Zhang, and B. P. T. Fokwa, "Boron-dependency of molybdenum boride electrocatalysts for the hydrogen evolution reaction," Angew. Chem., Int. Ed. **56**, 5575–5578 (2017).

[9] J. Masa, I. Sinev, H. Mistry, E. Ventosa, M. de la Mata, J. Arbiol, M. Muhler, B. Roldan Cuenya, and W. Schuhmann, "Ultrathin high surface area nickel boride (Ni_xB) nanosheets as highly efficient electrocatalyst for oxygen evolution," Adv. Energy Mater. **7**, 1700381 (2017).

[10] S. Klemenz, J. Schuch, S. Hawel, A.-M. Zieschang, B. Kaiser, W. Jaegermann, and B. Albert, "Synthesis of a highly efficient oxygen-evolution electrocatalyst by incorporation of iron into nanoscale cobalt borides," ChemSusChem **11**, 3150–3156 (2018).

[11] J. Masa, P. Weide, D. Peeters, I. Sinev, W. Xia, Z. Sun, C. Somsen, M. Muhler, and W. Schuhmann, "Amorphous cobalt boride (Co_2B) as a highly efficient nonprecious catalyst for electrochemical water splitting: Oxygen and hydrogen evolution," Adv. Energy Mater. **6**, 1502313 (2016).

[12] A.-M. Zieschang, J. D. Bocarsly, J. Schuch, C. V. Reichel, B. Kaiser, W. Jaegermann, R. Seshadri, and B. Albert, "Magnetic and electrocatalytic properties of nanoscale cobalt boride, Co_3B," Inorg. Chem. **58**, 16609–16617 (2019).

[13] K. Hofmann, N. Kalyon, C. Kapfenberger, L. Lamontagne, S. Zarrini, R. Berger, R. Seshadri, and B. Albert, "Metastable Ni_7B_3: A new paramagnetic boride from solution chemistry, its crystal structure and magnetic properties," Inorg. Chem. **54**, 10873–10877 (2015).

[14] N. Kalyon, K. Hofmann, J. Malter, M. Lucas, P. Claus, and B. Albert, "Catalytic activity of nanoscale borides: Co_2B and Ni_7B_3 in the liquid-phase hydrogenation of citral," J. Catal. **352**, 436–441 (2017).

[15] J. D. Bocarsly, E. E. Levin, S. A. Humphrey, T. Faske, W. Donner, S. D. Wilson, and R. Seshadri, "Magnetostructural coupling drives magnetocaloric behavior: The case of MnB versus FeB," Chem. Mater. **31**, 4873–4881 (2019).

[16] S. Ma, R. Farla, K. Bao, A. Tayal, Y. Zhao, Q. Tao, X. Yang, T. Ma, P. Zhu, and T. Cui, "An electrically conductive and ferromagnetic nano-structure manganese mono-boride with high Vickers hardness," Nanoscale **13**, 18570–18577 (2021).

[17] A. L. Bowman and N. G. Nereson, "Manganese boride, MnB_2," AIP Conf. Proc. **17**, 34–36 (1974).

[18] H. Gou, G. Steinle-Neumann, E. Bykova, Y. Nakajima, N. Miyajima, Y. Li, S. V. Ovsyannikov, L. S. Dubrovinsky, and N. Dubrovinskaia, "Stability of MnB_2 with AlB_2-type structure revealed by first-principles calculations and experiments," Appl. Phys. Lett. **102**, 061906 (2013).

[19] R. Kiessling, "The borides of manganese," Acta Chem. Scand. **4**, 209–227 (1950).

[20] A. Knappschneider, C. Litterscheid, N. C. George, J. Brgoch, N. Wagner, J. Beck, J. A. Kurzman, R. Seshadri, and B. Albert, "Peierls-distorted monoclinic MnB_4 with a Mn–Mn bond," Angew. Chem. **126**, 1710–1714 (2014).

[21] A. Knappschneider, C. Litterscheid, J. Brgoch, N. C. George, S. Henke, A. K. Cheetham, J. G. Hu, R. Seshadri, and B. Albert, "Manganese tetraboride, MnB_4: High-temperature crystal structure, p–n transition, ^{55}Mn NMR spectroscopy, solid solutions, and mechanical properties," Chem. Eur. J. **21**, 8177–8181 (2015).

[22] P. K. Liao and K. E. Spear, "The B–Mn (boron–manganese) system," Bull. Alloy Phase Diagrams **7**, 543–549 (1986).

[23] I. Smid, P. Rogl, and F. Weitzer, "The ternary system: Manganese–boron–nitrogen," in *Proceedings of the 12th International Plansee Seminar* (Reutte, Austria, 1989), Vol. 2, p. 577.

[24] L.-E. Tergenius, "Refinement of the crystal structure of orthorhombic Mn_2B (formerly denoted Mn_4B)," J. Less-Common Met. **82**, 335–340 (1981).

[25] B. Wang, X. Li, Y. X. Wang, and Y. F. Tu, "Phase stability and physical properties of manganese borides: A first-principles study," J. Phys. Chem. C **115**, 21429–21435 (2011).

[26] M. Fries, Z. Gercsi, S. Ener, K. P. Skokov, and O. Gutfleisch, "Magnetic, magnetocaloric and structural properties of manganese based monoborides doped with iron and cobalt—A candidate for thermomagnetic generators," Acta Mater. **113**, 213–220 (2016).

[27] S. Ma, K. Bao, Q. Tao, P. Zhu, T. Ma, B. Liu, Y. Liu, and T. Cui, "Manganese mono-boride, an inexpensive room temperature ferromagnetic hard material," Sci. Rep. **7**, 43759 (2017).

[28] X. Meng, K. Bao, P. Zhu, Z. He, Q. Tao, J. Li, Z. Mao, and T. Cui, "Manganese borides synthesized at high pressure and high temperature," J. Appl. Phys. **111**, 112616 (2012).

[29] T. Simsek and S. Özcan, "Influence of crystal size on the magnetic properties of manganese monoboride nanoparticles," IEEE Trans. Magn. **54**, 2301204 (2018).

[30] N. Lundquist and H. P. Myers, S. Aktiebolaget Atomenergi (Sweden, 1960), AE-46, 3–19.

[31] T. Shigematsu, T. Kanaizuka, K. Kosuge, M. Shiga, Y. Nakamura, and S. Kachi, "Thermal expansion anomaly of MnB," Phys. Lett. A **53**, 385–386 (1975).

[32] V. I. Timoshchuk, "The magnetic properties of single crystal MnB," Phys. Met. Metallogr. **59**, 179–181 (1985).

[33] G. Papesch, H. Nowotny, and F. Benesovsky, "Untersuchungen in den Systemen: Chrom-Bor-Kohlenstoff, Mangan-Bor-Kohlenstoff und Mangan-Germanium-Kohlenstoff," Monatsh. Chem. **104**, 933–942 (1973).

[34] S. Klemenz, M. Fries, M. Dürrschnabel, K. Skokov, H.-J. Kleebe, O. Gutfleisch, and B. Albert, "Low-temperature synthesis of nanoscale ferromagnetic α'-MnB," Dalton Trans. **49**, 131–135 (2020).

[35] S. Rades, A. Kornowski, H. Weller, and B. Albert, "Wet-chemical synthesis of nanoscale iron boride, XAFS analysis and crystallization to α-FeB," ChemPhysChem **12**, 1756–1760 (2011).

[36] S. Rades, S. Kraemer, R. Seshadri, and B. Albert, "Size and crystallinity dependence of magnetism in nanoscale iron boride, α-FeB," Chem. Mater. **26**, 1549–1552 (2014).

[37] F. Igoa Saldaña, E. Defoy, D. Janisch, G. Rousse, P.-O. Autran, A. Ghoridi, A. Séné, M. Baron, L. Suescun, Y. Le Godec, and D. Portehault, "Revealing the

elusive structure and reactivity of iron boride α-FeB," Inorg. Chem. **62**, 2073–2082 (2023).
[38] S. Kervan, "Magnetic properties of the MnB boride by density functional theory," J. Supercond. Nov. Magn. **24**, 815–818 (2011).
[39] J. Park, Y.-K. Hong, H.-K. Kim, W. Lee, C.-D. Yeo, S.-G. Kim, M.-H. Jung, C.-J. Choi, and O. N. Mryasov, "Electronic structures of MnB soft magnet," AIP Adv. **6**, 055911 (2016).
[40] Program Topas V4.2, Bruker AXS Karlsruhe, 2009.
[41] G. M. Sheldrick, "A short history of SHELX," Acta Crystallogr. A **64**(1), 112–122 (2008).
[42] Further details of the crystal structure investigation may be obtained from Fachinformationszentrum Karlsruhe, 76344 Eggenstein-Leopoldshafen, Germany [E-mail: crysdata@fiz-karlsruhe.de; Web: http://www.fiz-karlsruhe.de/request_for_deposited_data.html; Fax: (+49)7247-808-666] upon quoting the number CSD-2209853.
[43] T. Kanaizuka, "Phase diagram of pseudobinary CrB–MnB and MnB–FeB systems: Crystal structure of the low-temperature modification of FeB," J. Solid State Chem. **41**, 195–204 (1982).
[44] P. Morin, J. Pierre, D. Schmitt, and D. Givord, "A canted magnetic structure in an S-ion compound: GdMg," Phys. Lett. A **65**, 156–158 (1978).